Generating low-temperature glow discharge plasma in the atmospheric pressure helium after spark breakdown: Modelling plasma with the prescribed properties for biomedical applications

V. P. Demkin, S. V. Melnichuk, and A. V. Postnikov
Tomsk State University, 36 Lenin Ave., 634050 Tomsk, Russian Federation

(Received 24 May 2018; accepted 10 July 2018; published online 31 July 2018)

This paper concerns computational modelling of the low-temperature glow discharge plasma in the atmospheric pressure helium after spark breakdown and research on the dependence of a spatial distribution of plasma on the initial conditions of discharge and parameters of the external electric circuit. This study analysed the influence of the initial distribution of a space charge on the generation of the glow discharge plasma after the spark breakdown between flat electrodes by means of a 2D-axial symmetric model of the atmospheric pressure helium plasma in the drift-diffusion approximation. With the discharge current of 1–12 mA, the solution for a quasi-steady state of plasma is obtained. The dependence of a type of this discharge mode on the parameters of the external electric circuit and coefficient of the secondary cathode emission is studied. *Published by AIP Publishing.*
https://doi.org/10.1063/1.5041316

I. INTRODUCTION

Over the past decade, there has been increasing interest in the field of applied research and applications of cold non-equilibrium atmospheric pressure plasma in biomedicine.[1] This is associated with the results of the experiments on the interaction of plasma with biological systems, tissues, and cells employed in clinical practice. Nowadays, bactericidal properties of plasma are widely used for medical purposes for sterilising medical instruments, wound healing, blood coagulation, and treating infectious skin diseases.[2,3] Active charged and neutral particles formed in plasma interact with biological tissues at the molecular level having disinfecting and therapeutic effects. Integrating plasma technologies into clinical practice gave rise to the development of plasma medicine. The new field of medicine marries physics, fundamental medicine, and information technologies.[4] To date, the most important direction in the development of plasma medicine is the interaction of plasma with cell structures, which causes changes in permeability of cell walls, excites cells, and stimulates cell proliferation and tissue regeneration.[5] Despite an abundance of research in the field, biological and physical mechanisms of the interaction of plasma with living cells have not been sufficiently studied, which prevents further application of plasma.

One of the crucial factors in achieving the therapeutic effect of plasma processing of cell structures is a source of plasma. Devices based on nonequilibrium gas-discharge plasma generated in arc, spark, and HF-plasmatrons (Ref. 6), dielectric-barrier discharges (Ref. 3) under atmospheric pressure, and electron-beam plasmachemical reactors under medium pressures (Refs. 7 and 8) serve as plasma sources. Plasma mainly affects living things by the interaction of active particles generated in plasma—electrons, ions, free radicals, and short-wavelength radiation—which are catalysts of chemical processes and trigger further biochemical reactions in biological tissues accelerating therapeutic effects.[9] Generation of biologically active particles, their spatial distribution, and their interaction with cell structures depend on the methods for plasma generation, ways of its delivery to surfaces, and doses of their processing by plasma. Therefore, each case requires an adequate regime of discharge burning and gas composition. It must be taken into account when processing cell structures to increase their activity. The processing implies more thorough selection of a chemical composition of plasma and more delicate adjustment of the electrophysical parameters of a source than cell inactivation processes.

Although plasma technologies are deeply integrated into medical practice, a number of issues related to generation of active particles, mechanisms of their influence on biological tissues, and determination of plasma doses and their dependence on the kinetics of the active particles still remain unsolved.[10,11]

One of the promising sources of plasma is a glow discharge generated by an impulse spark discharge.[12–14] Using plasma sources based on the glow discharge maintained by its spark discharge gives an opportunity to obtain plasma jets with controllable concentrations of biologically active particles and intensity of the short-wavelength radiation spectrum, which is more promising for biomedical applications. However, understanding physical mechanisms of the energy transfer in the glow-to spark transition and controlling the parameters of non-steady plasma require a detailed mathematical model of this type of discharge.[9] Therefore, this study is aimed at modelling plasma with the prescribed parameters on the basis of glow-to-spark transition created in a non-steady low-current low-temperature plasmotron.[14]

Nowadays, there are a few methods and approaches to the solution to the problem based on analytical models, Boltzmann equation, kinetic equations, and statistical simulation.[15–19] The main disadvantage in plasma modelling for

biomedical applications is the inconsistency of these approaches providing the basis for the model that finally leads to the discrepancy between the available theoretical results and experimental data obtained by the corresponding methods of plasma diagnosis.

Reference 20 provides the results of calculations of the dynamics of the parameters of the atmospheric pressure helium plasma formed after the spark breakdown. The results obtained in that study for the conditions similar to Ref. 13 showed that the initial stage of the current development is impulse associated with the formation of a near-cathode layer of the discharge. Having passed through the current impulse, the discharge falls into the quasi-steady mode accompanied by the expansion of the near-cathode layer, which is determined by the presence of an uncompensated positive charge in the layer. The increase in the volume occupied by plasma is accompanied by the increase in the electric current and decrease in the voltage on the electrodes.

To get deeper insight into the development of the discharge and dependence of the parameters of the quasi-steady mode on the formation of the near-cathode layer (Ref. 13), we have studied the influence of the initial distribution of the space charge on the electrophysical characteristics of the discharge after the breakdown in the atmospheric pressure helium.

II. DISCHARGE MODEL

The calculation is based on the mathematical model of plasma presented in Ref. 20. The state of electron and ion components of plasma was calculated according to the continuity equations for electron density, electron volume energy density, and continuity equation for the density of heavy particles. The drift-diffusion approximation was used to find the vector of electron flux. The initial data on the densities of electrons and ions were taken to calculate the electric field of the discharge in view of the boundary conditions set by the configuration of the electrical circuit shown in Fig. 1(a). There is a power supply on the right in the electrical circuit with voltage $U0$ which inputs to the discharge gap shown on the left in the electrical circuit through resistance R. Capacitor C is set parallel to the discharge gap to form a current pulse.

The calculations were carried out under the following parameters of the electric circuit: $U0 = -1500$ V, $R = 100$, 200, and 300 kΩ, and $C = 0$ and 1 pF. The voltage $U0$ from the power supply was input through the resistance R on the flat cylindrical electrodes presented in Figs. 1(b) and 1(c). The diameter of the electrodes is $b = 6$ mm, and the distance between them is $a = 1$ mm. The figures demonstrate the initial distribution of the space charge of two types. In Fig. 1(b), the distribution corresponds to the electrically neutral homogeneous plasma column of the cylindrical shape with the diameter $d = 0.2$ mm and concentration of electrons and ions $n_e = n_i = 5 \times 10^{19}$ cm^{-3}.[20] The distribution simulates the initial state of plasma after passing a positive streamer or several spark breakdowns. Figure 1(c) illustrates the second type of distribution corresponding to the electrically neutral cylindrical layer in the near-cathode region with the diameter $d = 0.2$ mm and height $h = 0.08$ mm and concentration of charged particles $n_e = n_i = 5 \times 10^{19}$ cm^{-3}.[20] This distribution simulates the initial state of plasma which may appear, for example, after explosive processes and stain formation on the cathode.[13]

The calculations were made by means of the finite-difference method with the use of a rectangular grid shown in Fig. 1(d) with the alternating linear size S of the elements. In the near-cathode region, $S = 0.002$ mm, and in the central region, $S = 0.004$ mm. The number of elements was selected according to the sizes of plasma inhomogeneous areas determined by the length of the free path of electrons in ionization.

The plasma collision scheme applied to the solution of the continuity equations incudes the reactions presented in Table I, where the temperature of electrons T_e is given in

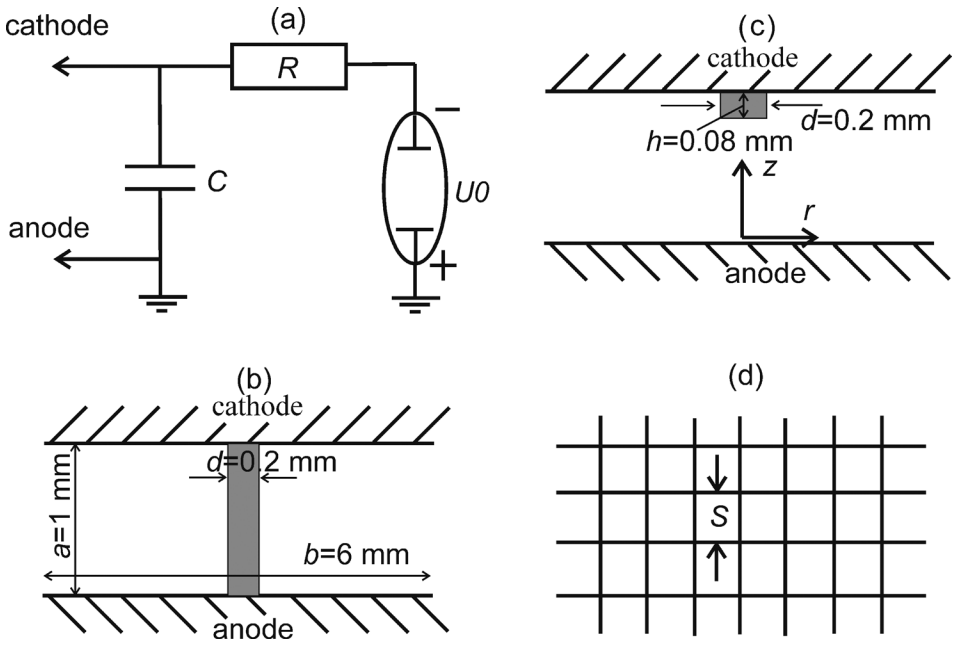

FIG. 1. (a) Electrical circuit of the discharge; (b) and (c) geometry of the initial conditions of the discharge; (d) grid of the finite-difference method.

TABLE I. Plasma collision scheme.

No.	Reaction	Velocity constant	References
1	$e + He => e + He$	$f(\varepsilon)$	21
2	$e + He => e + He^*$	$f(\varepsilon)$, $\Delta\varepsilon = 20$ eV	21
3	$e + He => 2{\cdot}e + He^+$	$f(\varepsilon)$, $\Delta\varepsilon = 25$ eV	21
4	$e + He^+ => He^*$	$6.67 \times 10^{-13} T_e^{-0.5}$ cm^3/s	22
5	$2{\cdot}e + He^+ => e + He$	$7.8 \times 10^{-38} (T_e/T_g)^{-4.4}$ cm^6/s	22
6	$e + He^+ + He => He^* + He$	$7.4 \times 10^{-35} (T_e/T_g)^{-2}$ cm^6/s	22
7	$e + He_2^+ => He^* + He$	$7.12 \times 10^{-15} (T_e/T_g)^{-1.5}$ cm^3/s	22
8	$2{\cdot}e + He_2^+ => e + He^* + He$	2.8×10^{-20} cm^3/s	22
9	$e + He_2^+ + He => He^* + 2{\cdot}He$	3.5×10^{-27} cm^6/s	22
10	$He^+ + 2{\cdot}He => He_2^+ + He$	$1.4 \times 10^{-31} (T_g/300)^{-0.6}$ cm^6/c	22

electron-volts and the temperature of gas T_g in Kelvins. Reactions 1–3 describe the elastic collision of electrons with gas atoms, integral excitation with the threshold value of energy $\Delta\varepsilon = 20$ eV and ionization c $\Delta\varepsilon = 25$ eV. The calculations of the processes were carried out according to the type of a cross-section and distribution of electrons between energies $f(\varepsilon)$. Reactions 4–9 refer to the recombination of charged particles. Reaction 10 demonstrates the formation of molecular ion He_2^+.

The calculation of the transport characteristics of the electron component was based on the data on the dependence of electrons mobility $\mu_e(\bar{\varepsilon})$ on their mean energy $\bar{\varepsilon}$ obtained in the numerical solution of the Boltzmann equation for various uniform electric fields. The type $\mu_e(\bar{\varepsilon})$ is presented in Fig. 2. The continuous part of the curve represents the data obtained as a result of the numerical calculation, whereas the dotted part of the curve shows the extrapolated values $\mu_e(\bar{\varepsilon})$ in the region of higher values $\bar{\varepsilon}$.

The mobility of He^+ and He_2^+ was taken from Ref. 23 and assumed to be 1.482×10^{-3} m^2/(V s) and 2.403×10^{-3} m^2/(V s), respectively.

The initial conditions of the discharge were selected assuming that after the spark breakdown, a compensated space charge appears, see Figs. 1(b) and 1(c). Capacitance C is charged up to the value $U0$; the electric field between the cathode and the anode is uniform, and its value is $E = U0/a = 1.5 \times 10^4$ V/cm. Pressure $P = 760$ Torr and temperature $T = 300$ K of gas were considered constant through the entire time interval.

On the boundary of discharge plasma region, it was assumed that the fluxes of charged and neutral particles perpendicular to the discharge auis turn zero The coefficient of the secondary emission of electrons from the cathode under the influence of ions was supposed to be $\gamma = 0.4$. The initial energy of primary and secondary electrons was assumed to be 4 eV and 1 eV, respectively.

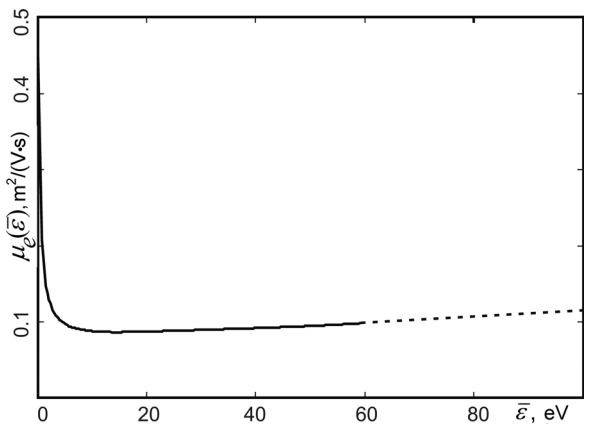

FIG. 2. Dependence of electron mobility μ_e on their mean energy $\bar{\varepsilon}$ in atmospheric pressure helium.

III. CALCULATION RESULTS

Figure 3(a) illustrates time-dependences of the currents I_b and I_c of the discharge, calculated for the initial conditions of the space charge distributions according to Figs. 1(b) and 1(c) at $R = 100$ kΩ and C = 0 pF. If C = 0 pF, the curves of current and voltage resemble each other. Figure 3 clearly demonstrates the significant difference in the dynamics of currents I_b and I_c at t $< 10^{-8}$ s, which is determined by the selection of the initial space charge distribution in the interelectrode gap. Under the equal space charge distribution in the plasma column [Fig. 1(b)] between the electrodes, the current I_b immediately differs from zero and increases by the time $t = 10^{-8}$ s with little dynamics. In the distribution of the space charge shown in Fig. 1(c), at the initial moment of time, there is no negative charge near the anode and $I_b \approx 0$ A is absent. As the electrons move from the cathode to the anode, their concentration grows.

Figure 3(b) shows the dynamics of the electric field E near the anode caused by this process. From the moment $t = 1.5 \times 10^{-9}$ s, increasing the concentration of electrons and electric field near the anode leads to a jump in the anode current and starts fading after that. As Fig. 3 demonstrates,

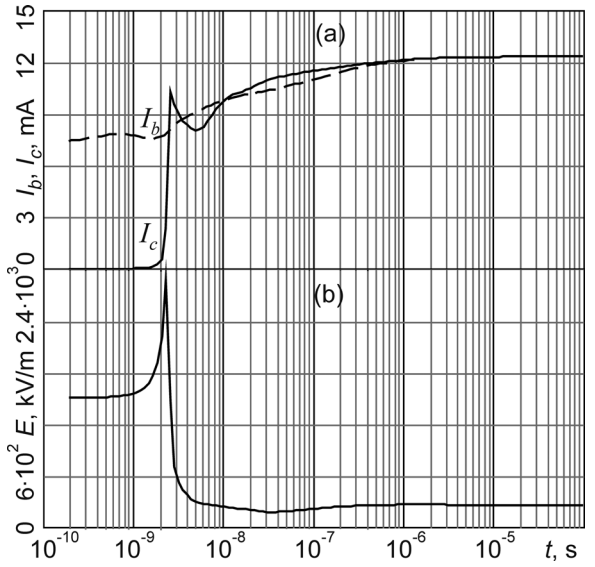

FIG. 3. (a) Dependence of the discharge currents I_b and I_c on time t under different initial conditions for $R = 100$ kΩ and C = 0 pF. (b) Dependence of the voltage of electric field E on time t near the anode corresponding to the current I_c.

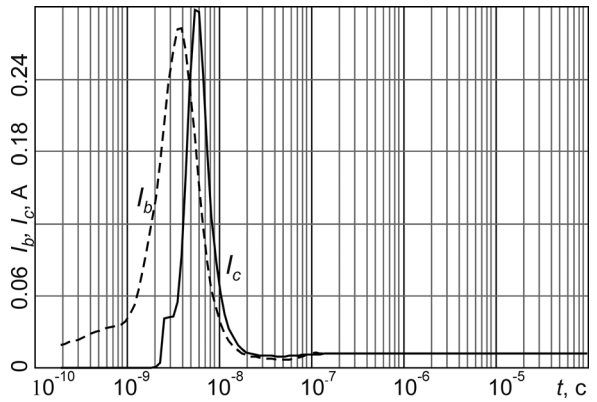

FIG. 4. Dependence of the discharge currents I_b and I_c on time t at different initial conditions for $R = 100\,\text{k}\Omega$ and $C = 1\,\text{pF}$.

the decrease in the electric current I_c is associated with the change in dynamics of the electric field intensity near the anode, which also starts fading as electrons move to the anode. Then, the value of the electric field is set lower than the original value due to the screening effect of the uncompensated positive charge near the cathode. Similar calculations at $C = 1\,\text{pF}$ also showed the difference in the dynamics of electrical currents I_b and I_c shown in Fig. 4. It can be clearly seen that in both cases, the current is impulse determined by the processes in the near-cathode layer (Ref. 20). The current I_c lags behind I_b and there is a shear in the leading edge of the I_c pulse.

The differences in the distribution of the concentration of electrons in Figs. 5(a) and 5(b) are caused by different initial conditions of the discharge development illustrated in Figs. 1(b) and 1(c). Figure 5(a) corresponds to the original distribution of the electrically neutral homogeneous cylindrical column of plasma spread over the entire interelectrode gap, whereas in Fig. 5(b), the electrically neutral plasma column is concentrated near the cathode only.

In Fig. 6(a), curves 1 and 2 show the distribution of the concentration of the uncompensated charge along the discharge radius in the middle of the interelectrode gap, corresponding to the data in Figs. 5(a) and 5(b). According to the curves, the periphery of the discharge is occupied by the uncompensated positive charge which creates a positive radial component of the electric field strength shown in Fig. 6(b). The presence of this component of the electric field along the plasma column limits the drift of electrons from the plasma volume.

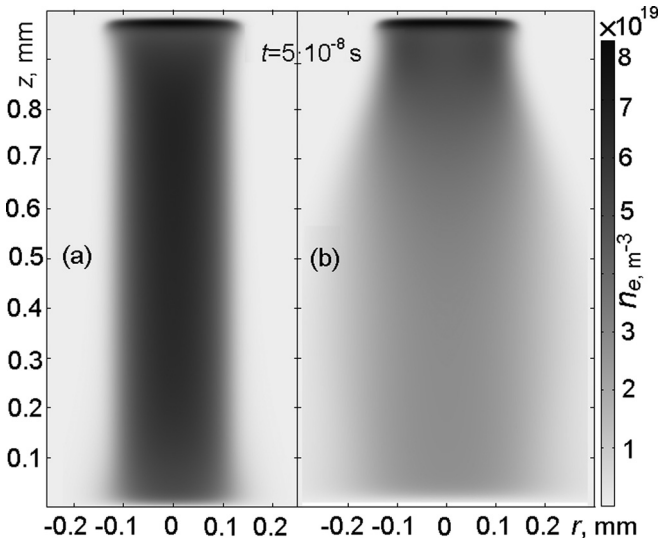

FIG. 5. Distribution of the concentration of electrons n_e in a space charge for $t = 5 \times 10^{-8}$ s at different initial conditions.

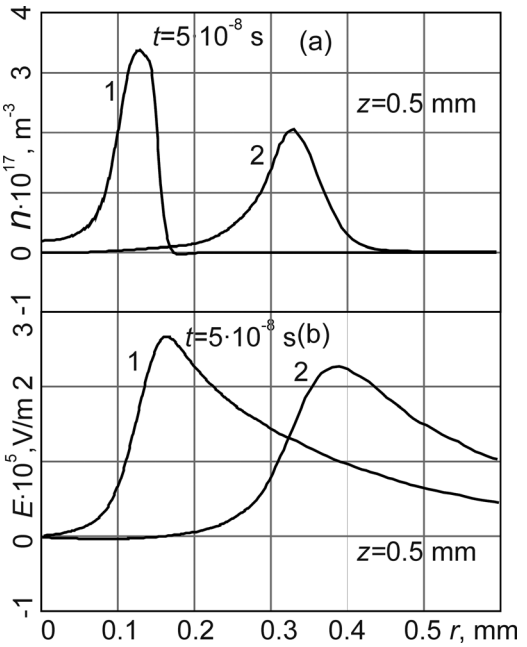

FIG. 6. (a) Distribution of the concentration n of the uncompensated charge along the discharge radius at z = 0.5 mm. (b) Distribution of the radial component of the electric field E along the discharge radius at z = 0.5 mm, corresponding to the initial data: curve 1—Fig. 5(a) and curve 2—Fig. 5(b).

In Fig. 7, curves 1 and 2 illustrate the distribution of the potential U on the discharge axis, corresponding to the initial data in Figs. 5(a) and 5(b). The potential difference between the cathode and the anode in these cases is $-440\,\text{V}$ and $-370\,\text{V}$. According to curves 1 and 2 in Fig. 7, by the time $t = 5 \times 10^{-8}$ s, the discharge corresponding to the initial conditions in Fig. 1(c) flows at the lower electric field strength in the region of the positive column (curve 2).

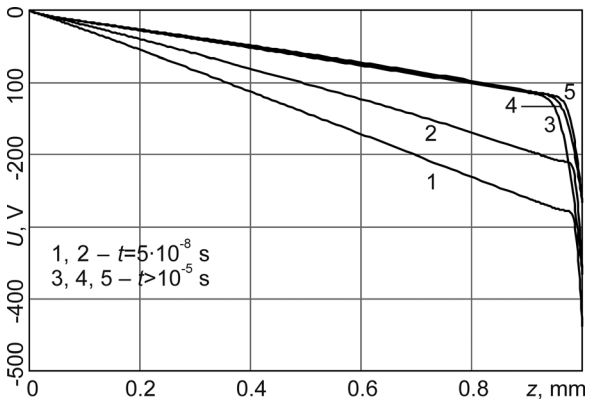

FIG. 7. Distribution of the potential U on the discharge axis: curves 1 and 2 correspond to the initial data in Figs. 5(a) and 5(b), respectively; curves 3, 4 and 5 correspond to $t > 10^{-5}$ s for $\gamma = 0.4$, $R = 300\,\text{kOm}$, $\gamma = 0.4$, $R = 200\,\text{kOm}$, $\gamma = 0.1$, $R = 100\,\text{kOm}$, respectively.

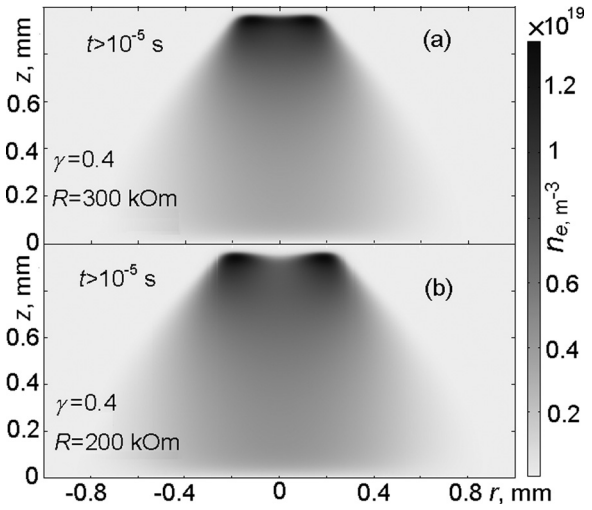

FIG. 8. Distribution of the concentration of electrons in the quasi-steady mode of the discharge: (a) at R = 300 kΩ and $\gamma = 0.4$ and (b) at R = 200 kΩ and $\gamma = 0.4$.

The uncompensated positive charge in the near-cathode region leads to its expansion.[20] The increase in the volume occupied by the discharge at $t > 10^{-7}$ s is accompanied by the increase in the electric current and decrease in the potential difference between the electrodes (Figs. 3 and 4). The magnitude of the longitudinal component of the electric field decreases both in the near-cathode layer and in the positive column, where it is much less.

As the calculations showed, at $t > 10^{-5}$ s, the expansion of the discharge volume stops and it becomes quasi-steady. The type of a quasi-steady discharge depends on the selected initial distribution of the concentration of charged particles and value of capacitance C. For a quasi-steady mode of the discharge, Figs. 8(a) and 8(b) describe the calculated distribution of the concentration of electrons in the discharge volume for $R = 300$ and 200 kΩ at the coefficient of secondary emission $\gamma = 0.4$. Figures 9(a) and 9(b) represent the similar distribution for $R = 100$ kΩ and $\gamma = 0.4$ and 0.1. The

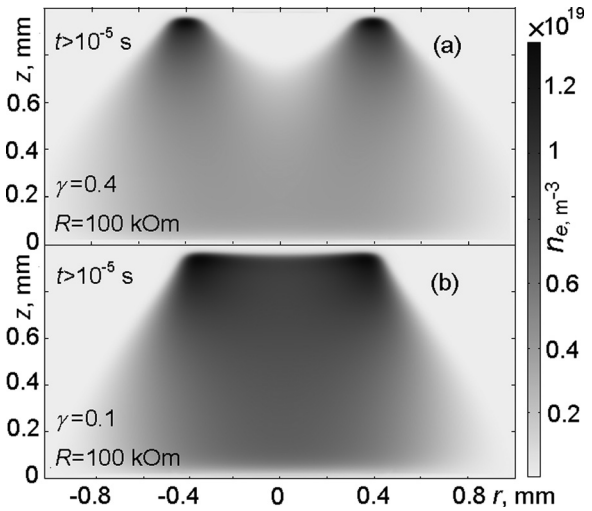

FIG. 9. Distribution of the concentration of electrons in the quasi-steady mode of the discharge: (a) at R = 100 kΩ and $\gamma = 0.4$ and (b) at R = 100 kΩ and $\gamma = 0.1$.

distribution of the potential along the discharge axis for Figs. 8(a), 8(b), and 9(b) is shown in Fig. 6 with curves 3, 4, and 5, respectively. For these curves, the potential difference between the electrodes makes up 270, 270, and 360 V, and the discharge current is 4.1 mA, 6.2 mA, and 11.4 mA. For Fig. 9(a), the potential difference between the electrodes is 270 V and the discharge current is 12.5 mA.

According to the results, within the quasi-steady mode of the discharge with $\gamma = 0.4$, when R decreases, the radial size of the near-cathode region increases along with the electric current of the discharge, whereas the potential difference between the electrodes remains the same. Curves 3, 4, and 5 in Fig. 6 show that in the quasi-steady mode, the distribution of the potential U in the region of the positive column is the same for the specified cases. Figure 9(a) shows that at $R = 100$ kΩ, due to the expansion of the near-cathode layer, its destruction occurs in the central region of the discharge. According to Fig. 5, curve 5, and Fig. 9(b), a decrease in γ to 0.1 leads to an increase in the voltage between the electrodes and the recovery of the near-cathode layer.

For $R = 100$ kΩ and $\gamma = 0.4$, Fig. 10(a) shows the distribution of the potential U in the near-cathode region ($z = 0.98$ mm) along the radius r for $t = 5 \times 10^{-8}$ s, corresponding to the stage of its expansion, and for $t > 10^{-5}$ s, which is a quasi-steady stage of the discharge. Figure 10(b) presents the distribution of the normalised per unit of the concentration of the uncompensated positive n_i charge along r at $z = 0.98$ mm for the same moments in time. According to the type of U for $t = 5 \times 10^{-8}$ s in Fig. 10(a), at the stage of the discharge expansion, the radial component of the electric

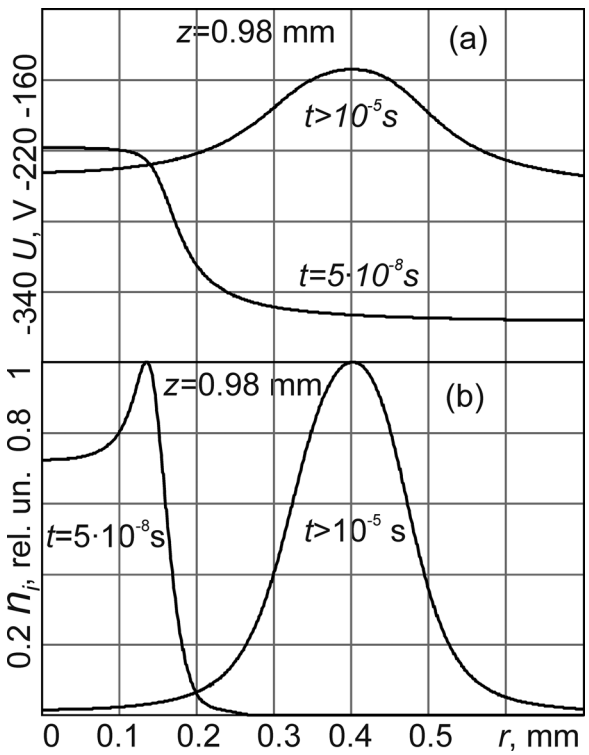

FIG. 10. (a) Distribution of the potential at $z = 0.98$ mm along the discharge radius r for $t = 5 \times 10^{-8}$ s and $t > 10^{-5}$ s. (b) Distribution of the normalised per unit of concentration of the uncompensated positive charge n_i at $z = 0.98$ mm along r for $t = 5 \times 10^{-8}$ s and $t > 10^{-5}$ s.

field in the entire near-cathode region is positive and dramatically increases towards its periphery contributing to the discharge expansion. When the discharge goes into the quasi-steady mode, the central region of the near-cathode region sees the decrease in the concentration of the uncompensated positive charge n_i [Fig. 10(b)]. As it can be seen in Fig. 10(a), for $t > 10^{-5}$ s, it leads to changes in the U distribution along r, corresponding to the emergence of a negative radial component of the electric field in the central region of the near-cathode layer. The component disappears towards the discharge axis and its periphery. In the region $r = 0.4$ mm, the radial component turns zero. As r grows, it becomes positive. Thus, in the transition to the quasi-steady stage, the peripheral region of the near-cathode layer ends up in the radial electric field changing the sign, which prevents the expansion of the volume occupied by the discharge. It can be seen in Fig. 11(a) that, in the quasi-steady mode of the discharge, in transition to the centre of the interelectrode gap ($z = 0.5$ mm), the uncompensated charge near the discharge axis becomes negative. As r grows, it becomes positive. The radial component of the electric field in this case [Fig. 11(b)] behaves similarly to the field in the near-cathode region, where it changes its direction as r grows.

IV. CONCLUSION

This paper considers the numerical modelling with the use of a 2D-axial symmetric model and study on the low-temperature glow discharge plasma in the atmospheric pressure helium after the spark breakdown and dependence of the discharge on the initial conditions and parameters of the external electric circuit.

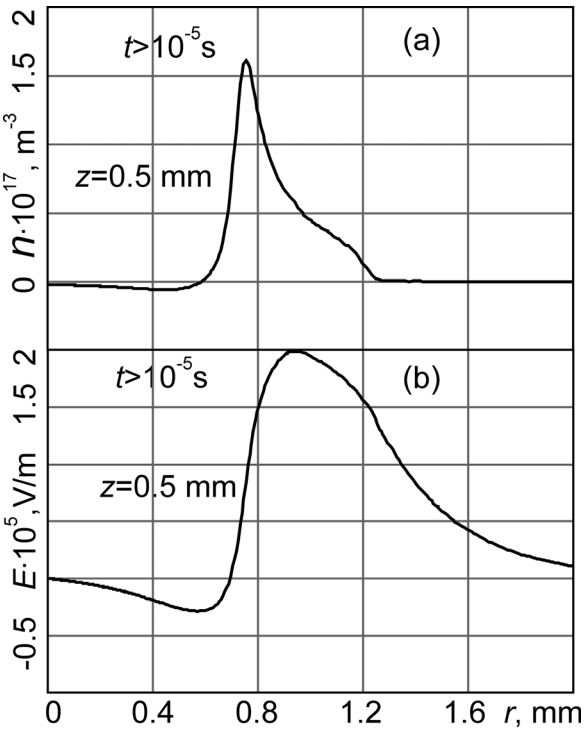

FIG. 11. (a) Distribution of the total charge n at $z = 0.5$ mm along the discharge radius r for $t > 10^{-5}$ s. (b) Distribution of the radial component of the electric field strength E at $z = 0.5$ mm for $t > 10^{-5}$ s.

The numerical calculations showed that setting the initial conditions of the distribution of the space charge both as a homogenous column in the entire interelectrode gap and as a narrow layer near the cathode leads to the development of a discharge with further transition to the quasi-steady mode with similar electrophysical characteristics. The comparative analysis of these calculations showed that the presence of a thin layer of an excess charge near the cathode manifests itself in the form of a sharp change in the electric current caused by the arrival of an electron avalanche from the cathode to the anode. It is shown that the initial distribution of the concentration of charged particles in the form of a homogeneous plasma column between the electrodes further limits the speed of its expansion. The transition of the discharge to the quasi-steady mode is accompanied by the termination of the expansion of the discharge channel caused by the change in the sign of the radial component of the vector of the electric field intensity with the increase in the distance from the discharge axis. The increase in the discharge current at the same difference of the potentials between the electrodes occurs due to the increase in the volume occupied by the discharge when the parameters of the electric circuit change. As the coefficient of the secondary emission of electrons from the cathode decreases, the near-cathode potential drop increases. The distribution of the potential in the region of the positive column along the discharge axis does not change. The increasing electrical field strength in the near-cathode region contributes to the maintenance of the discharge at the lower coefficient of the secondary emission due to the increase in the electric field and concentration of positively charged particles.

According to the calculations, after the spark breakdown, at the initial stage of discharge, the uncompensated positive charge and larger longitudinal component of the electric field intensity form in its volume. In the transition to the quasi-steady mode of the discharge, when the radial component of the electric field intensity prevails, plasma becomes more electro-neutral.

ACKNOWLEDGMENTS

This work was supported by The Tomsk State University competitiveness improvement programme under Grant (No. 8.1.21.2018).

[1]M. Laroussi and X. Lu, J. Appl. Phys. **122**, 020901 (2017).
[2]G. Fridman, G. Friedman, A. Gutsol, A. B. Shekhter, V. N. Vasilets, and A. Fridman, Plasma Processes Polym. **5**, 503 (2008).
[3]D. B. Graves, Phys. Plasmas **21**, 080901 (2014).
[4]M. R. Wertheimer and S. Coulombe, Phys. Can. **68**(4), 189 (2012).
[5]K.-D. Weltmann and Th. von Woedtke, Plasma Phys. Controlled Fusion **59**(1), 014031 (2017).
[6]Th. Von Woedtke, H.-R. Metelmann, and K.-D. Weltmann, Contrib. Plasma Phys. **54**(2), 104 (2014).
[7]P. A. Bokhan and D. E. Zakrevsky, Tech. Phys. Lett. **28**(11), 21 (2002).
[8]V. P. Demkin, H. Kingma, R. Van De Berg, S. V. Melnychuk, O. V. Demkin, M.-S. Herards, V. S. Ripenko, and K. A. Sitnik, Russ. Phys. J. **58**(5), 740 (2015).
[9]V. P. Demkin, S. V. Melnychuk, O. V. Demkin, H. Kingma, and R. Van De Berg, Phys. Plasmas **23**(4), 043509 (2016).
[10]I. P. Ivanova, S. V. Trofimova, N. Karpel Vel Leitner, N. A. Aristova, E. V. Arkhipova, O. E. Burkhina, V. A. Sysoeva, and I. M. Piskarev, Sovrem. Tehnol. Med. **2**, 20 (2012).

[11]K. A. Astafyeva and I. P. Ivanova, Clin. Med. **9**(1), 115 (2017).
[12]Y. D. Korolev, O. B. Frants, N. V. Landl, and A. I. Suslov, IEEE Trans. Plasma Sci. **40**(11), 2837 (2012).
[13]Y. D. Korolev, O. B. Frants, V. G. Geyman, V. S. Kasyanov, and N. V. Landl, IEEE Trans. Plasma Sci. **40**(11), 2951 (2012).
[14]Y. D. Korolev, O. B. Frants, N. V. Landl, V. G. Geyman, and I. B. Matveev, IEEE Trans. Plasma Sci. **37**(4), 586 (2009).
[15]B. M. Smirnov, Phys. Usp. **52**, 559 (2009).
[16]A. Bogaerts, R. Aerts, R. Snoeckx, W. Somers, W. Van Gaens, M. Yusupov, and E. Neyts, J. Phys.: Conf. Ser. **399**, 012011 (2012).
[17]G. E. Georghiou, A. P. Papadakis, R. Morrow, and A. C. Metaxas, J. Phys. D: Appl. Phys. **38**(20), R303 (2005).
[18]N. Balcon, G. J. M. Hagelaar, and J. P. Boeuf, IEEE Trans. Plasma Sci. **36**(5), 2782 (2008).
[19]A. J. Yang, X. H. Wang, M. Z. Rong, D. X. Liu, F. Iza, and M. G. Kong, Phys. Plasmas **18**, 113503 (2011).
[20]V. P. Demkin and S. V. Melnichuk, Russ. Phys. J. **60**, 339 (2017).
[21]V. P. Demkin and S. V. Melnichuk, Phys. Plasmas **21**, 093504 (2014).
[22]D. X. Liu, P. Bruggeman, F. Iza, M. Z. Rong, and M. G. Kong, Plasma Sources Sci. Technol. **19**(2), 025018 (2010).
[23]X. Yuan and L. L. Raja, IEEE Trans. Plasma Sci. **31**(4), 495 (2003).